Ultrasonic spectroscopy of complex media

J. H. Page

Department of Physics and Astronomy
University of Manitoba
Winnipeg, MB Canada R3T 2N2

Summary. — Mesoscopic wave physics underpins many of the new developments in ultrasonic spectroscopy for probing the physical properties of complex heterogeneous materials. In this paper, two examples of recent progress are summarized. The first is Diffusing Acoustic Wave Spectroscopy (DAWS), which is a powerful approach for investigating the dynamics of strongly scattering media, one example being velocity fluctuations in fluidized suspensions of particles. Recent advances in using phase statistics to probe the particle dynamics are shown to give increased sensitivity in some situations; this work has also led to new insights into the meaning of phase for multiply scattered waves. The second topic is the spectroscopy of soft food biomaterials, illustrated by experimental studies of ultrasonic velocity and attenuation in bread dough. Since wheat flour dough contains one of the strongest scatterers of ultrasonic waves (bubbles) dispersed in a viscoelastic matrix that is also very dissipative, appropriate ultrasonic techniques provide an excellent means for investigating its structure and dynamics. In addition to fundamental studies, unraveling the contributions of bubbles and matrix to dough properties is relevant to the baking industry, because the bubbles ultimately grow into the voids that determine the structural integrity of bread – an important quality attribute. The interpretation of ultrasonic experiments on bread dough over three decades in frequency is giving new insights into this complex material, as well as providing the basis for new non-destructive methods of evaluating both dough processing behaviour and the breadmaking potential of different flours.

1. – Introduction

The fundamental studies of ultrasonic wave transport in strongly scattering random media, described in refs. [1, 2, 3, 4, 5], have facilitated the development of ultrasonic techniques for probing the physical properties of complex materials. Many such materials are mesoscopic, with internal structures on length scales comparable with ultrasonic wavelengths, and it is the structure and dynamics at this mesoscopic scale that determine their macroscopic physical properties. Familiar examples include foams, gels, slurries and a wide range of food biomaterials, all of which are playing an increasing important role in industrial applications, and hence our prosperity. Mesoscopic structure, however, often leads to multiple scattering of ultrasound, making traditional imaging methods impossible and motivating the development and application of new approaches for extracting useful information.

This paper reviews two examples of ultrasonic spectroscopy and their application to novel materials characterization methods. The next section outlines Diffusing Acoustic Wave Spectroscopy (DAWS), a powerful technique in field fluctuation spectroscopy for investigating the dynamics of strongly scattering media. Differences with the complementary technique of Diffusing Optical Wave Spectroscopy are discussed, highlighting the advantages of DAWS in some contexts. DAWS is illustrated with experiments on suspensions of particles and bubbles. Recent progress in probing dynamic properties using the phase of multiply scattered waves, which can readily be measured for ultrasound but less easily for light, is summarized. Diffusing Acoustic Wave Spectroscopy, introduced in 2000 [6] and described in detail in ref. [7], has also been reviewed in ref. [8], and more recently in a broader context in Physics Today [9]. The interested reader is encouraged to consult these references for additional information.

Section **3** illustrates the characterization of food materials using ultrasound. Many food materials are both strongly scattering and strongly absorbing for ultrasound, and in cases where the multiple scattering coda is suppressed by dissipation, it is not feasible to use techniques such as DAWS to probe their evolution during processing. Nonetheless information on the mechanical properties of foods is important in the preparation and production of foods with appealing texture, which is crucial for making foods palatable to eat. This information can be obtained from spectroscopic techniques that rely on ballistic propagation, and are especially valuable when data over a wide range of ultrasonic frequencies are available. This approach is illustrated with experiments on bread dough [10, 11, 12, 13, 14, 15, 16, 17, 18, 19], where processing challenges encountered when incorporating nutritional supplements may make ultrasonic monitoring techniques of particular value to the functional foods industry.

(*) Published in the Proceedings of the International School of Physics Enrico Fermi, Course CLXXIII, "Nano Optics and Atomics: Transport of Light and Matter Waves", edited by R. Kaiser, D.S. Weirsma and L. Fallani (IOS, Amsterdam; SIF, Bologna, 2011) pp. 115-131. The original publication is available from SIF at http://www.sif.it/SIF/en/portal/books/series/rendiconti_fermi.

2. – Diffusing Acoustic Wave Spectroscopy

Diffusing Acoustic Wave Spectroscopy (DAWS) determines the dynamics of a strongly scattering medium from the temporal fluctuations of ultrasonic waves that are scattered many times before leaving the medium [6, 7]. Because multiply scattered waves are used, the technique is extremely sensitive to the motion of the scatterers in the medium, or to the evolution of the properties of the host material in which the scatterers are located; this sensitivity results from the large number of scattering events that are involved, leading to long trajectories over which cumulative changes in the detected waves occur. As the name suggests, there is much in common with the analogous technique of Diffusing Optical Wave Spectroscopy (often simply abbreviated DWS) [20, 21], although there are differences in the way in which the measurements are made and in the range of applications for which the two techniques are well suited. One advantage of DAWS is that the scattered wave field is measured, not the intensity, so that the field correlation function $g_1(\tau)$ is determined directly. Thus, there is no need to invoke the Siegert relation to interpret measurements of intensity correlation functions using models for the field correlation functions. Another advantage of detecting the wave field in DAWS is that the phase of the scattered fields can be exploited, offering the potential of better sensitivity in some cases. The other major technical difference is the ease with which pulsed measurements can be performed, enabling the detected changes to be monitored for a fixed path length of the multiply scattered waves and therefore simplifying the analysis. Finally, since ultrasonic wavelengths and wave periods are both larger (typically ~ 1 mm and 1 μs), DAWS is sensitive to dynamics on longer length scales than is possible with light (or x rays), enabling different types of materials and phenomena to be investigated. By varying the frequency, this range of length scales can be extended significantly, and can range up to kilometres for seismic applications.

Figure 1 shows two contrasting examples of evolving multiply scattered wave fields that can be used to probe changes in the system under investigation. Figure 1(a) shows a typical experimental setup in DAWS, where a pulsed incident wave from a generating transducer propagates through a sample containing moving particles or bubbles (fig. 1(b)) and is detected by a hydrophone. A typical multiple scattering path is indicated by the red arrows. Two segments of the transmitted field are shown in fig. 1(c), showing that at early propagation times, almost no change in the transmitted field is seen, while at later times, the wave field changes significantly as the scatterers move. Note that there are two relevant times in this problem, the propagation time t of the waves in the medium, which sets the sensitivity, and the evolution time T, which sets the time scale over which the dynamics are recorded. In DAWS, the medium can be interrogated repeatedly on a scale set by the pulse repetition time ΔT, which can be varied over a wide range to match the rate at which the system is evolving; in this case, $T = m\Delta T$, where m is an integer. Figure 1(c) shows that the waves are decorrelated in *both* amplitude and phase as the evolution time increases, due to the motion of the bubbles in the suspension. Analysis of the detected field fluctuations can be used to probe the velocities of the bubbles. By contrast, the changes in the waveforms shown in fig. 1(d), which were detected on

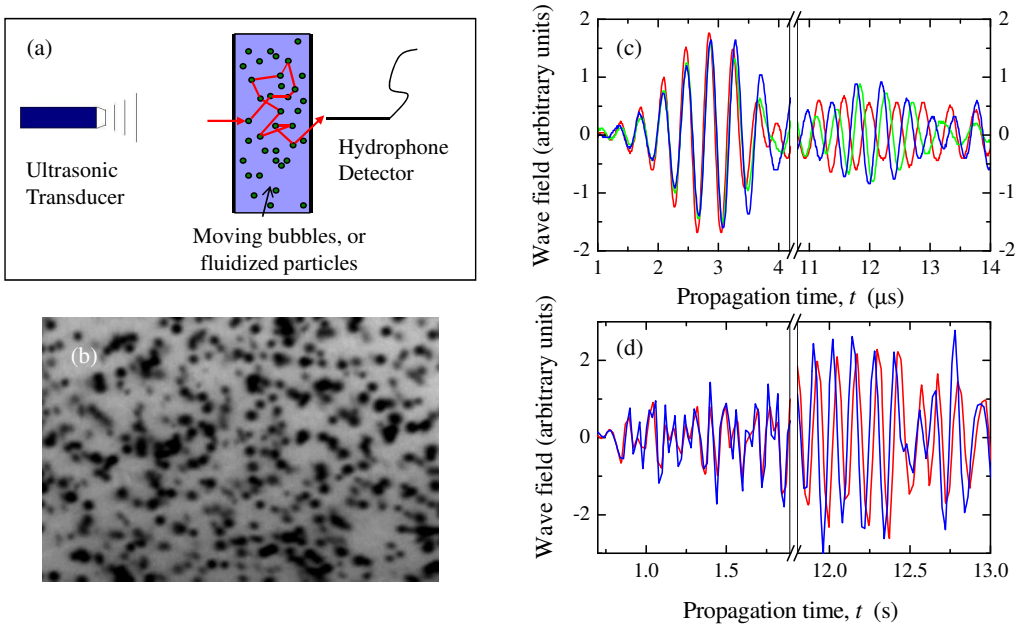

Fig. 1. – (a) Typical setup for measuring the dynamics of fluidized suspensions or bubbles using Diffusing Acoustic Wave Spectroscopy. The red arrows indicate a multiple scatttering path through the sample. (b) Photograph of $\sim$ 20-μm-diameter bubbles generated by an electrolysis technique. These small bubbles move in complex swirling patterns through water. (c) Two segments of the scattered wave fields transmitted through a fluidized suspension of glass particles, observed at three evolution times separated by 60 ms. The waveforms are very similar at early propagation times, but exhibit large fluctuations in both phase and amplitude a later times. (d) Waveforms detected by a seismograph on Mount Merapi, the site of an active volcano in Indonesia, after an air gun was used to generate short low frequency pulses 2 km away. The evolution time interval between the two recorded signals (red and blue traces) is two weeks. The shift in the phase of the waves can be most simply measured from a windowed cross correlation function of the fields at the two times; this phase shift is related to a small change in the seismic velocity, as explained in ref. [9].

Mount Merapi by a seismograph located 2 km away from the source, at evolution times separated by two weeks, are shifted in propagation time but remain similar otherwise. In this case, there is a uniform change in the medium, and the phase shift is related to a change in the seismic wave speed.

To determine the changes in the medium from the evolution of the scattered wave fields, it is helpful to describe the multiply scattered waves detected at propagation time t and evolution time T as the superposition of waves that have propagated along each scattering path p. This can be shown explicitly by writing the measured field $\psi(t, T)$ as

the real part of a complex field (the complex analytic signal)

$$\Psi(t,T) = A(t,T)e^{i[\omega t+\Phi(t,T)]} = \sum_p a_p(t,T)e^{i[\omega t+\phi_p(t,T)]} \,. \tag{1}$$

Here ω is the central frequency of the pulse, $\Phi(t,T)$ is the total phase of the scattered waves at the detector and $\phi_p(t,T)$ is the phase along a single multiple scattering path, which may be conveniently called the "path phase". As the medium evolves in time, the waves still propagate along these scattering paths, but the path lengths change, so that ψ is a function of both propagation time t and evolution time T. One direct way of relating the changes in $\psi(t,T)$ to the dynamics of the medium is to take the autocorrelation function of the field at a fixed propagation time t_s, thereby selecting multiple scattering paths with an average length $s = t_s/v_E$ and a narrow path length range determined by the source pulse width. The field autocorrelation function $g_{1,t_s}(\tau)$ is

$$g_{1,t_s}(\tau) = \frac{\int \psi(T)\ \psi(T+\tau)\, dT}{\int |\psi(T)|^2 dT} \simeq \left\langle e^{-i\,\Delta\phi_p(\tau)} \right\rangle, \tag{2}$$

where $\Delta\phi_p(\tau)$ is the change in phase of a path containing n scattering events during the evolution time interval τ. Here $n = v_E t_s/l^*$, where v_E and l^* are the transport velocity and mean free path of the multiply scattered waves. In general, the phase change for each path can be written as the sum of the ensemble average phase shift $\langle\Delta\phi_{\rm path}(\tau)\rangle$ and the deviation from the average value $\delta\phi_{\rm path}(\tau)$, enabling the autocorrelation function (2) to be written as a product of two factors, involving the average phase shift and its variance respectively:

$$g_{1,t_s}(\tau) \simeq \cos\left(\langle\Delta\phi_{\rm path}(\tau)\rangle\right) \exp\left(-\frac{1}{2}\left\langle\delta\phi^2_{\rm path}(\tau)\right\rangle\right). \tag{3}$$

To obtain this result, the contribution to g_1 from the ensemble average of $\left\langle e^{-i\,\delta\phi_{\rm path}(\tau)}\right\rangle$ is obtained to leading order using a cumulant expansion [6, 7, 8], and the real part of g_1 is taken, since this corresponds to the experimental situation.

A nonzero average phase shift arises when there is a uniform dilation of the medium seen by the waves, such as can occur if there is a change in wave velocity, which shifts the arrival time of all the scattered waves in the same way (e.g., see fig. 1(d)). In the case of a small wave velocity change Δv, $\langle\Delta\phi\rangle = -\omega t\Delta v/v$, where ω is the angular frequency.

When the scatterers are moving, such as for the example of moving bubbles in fig. 1(b),(c), the dominant contribution to the decay of g_1 comes from the path phase variance $\left\langle\delta\phi^2_{\rm path}\right\rangle$. In this case, the path phase variance can be related to the phase fluctuations for each step j along a path, which are given by $\vec{k}_j \cdot \Delta\vec{r}_{{\rm rel},j}$ where $\vec{k}_j$ is the wave vector of the wave scattered between the j^{th} to the $(j+1)^{th}$ scatterers, and $\Delta\vec{r}_{{\rm rel},j}$ is their relative displacement [6, 7, 8]. When the successive phase shifts along the paths,

as well as the directions of $\vec{k}_j$ and $\Delta\vec{r}_{\mathrm{rel},j}$, are uncorrelated, the field autocorrelation function is given by

$$g_{1,t_s}(\tau) \approx \exp\left[-\frac{nk^2}{6}\left\langle \Delta r^2_{\mathrm{rel}}(\tau, l^*)\right\rangle\right]. \tag{4}$$

(Here the average phase shift in eq. 3 has been set to zero, as is observed for fluidized particles; then, $\left\langle \delta\phi^2_{\mathrm{path}}\right\rangle = \left\langle \Delta\phi^2_{\mathrm{path}}\right\rangle$). This equation shows that the decay of the correlation function is determined by the relative mean square displacement of the scatterers that are separated, on average, by the average step length of the multiply scattered waves, l^*. Measuring the field autocorrelation function thus enables the relative motion of the scatterers to be determined on a length scale that can be tuned by the ultrasonic frequency.

Typical DAWS results for the dynamics of fluidized particles, suspended by flowing the liquid upwards to counteract sedimentation, are shown in fig. 2. In this example, the scatterers are 1-mm-diameter glass spheres surrounded by a liquid mixture of water and glycerol. At short evolution times, the motion of the particles is ballistic since the relative mean square displacement grows quadratically with time, $\left\langle \Delta r^2_{\mathrm{rel}}(\tau, l^*)\right\rangle = \left\langle \Delta V^2_{\mathrm{rel}}(l^*)\right\rangle \tau^2$, allowing the variance in the relative particle velocities to be measured directly from the slope of $\left\langle \Delta r^2_{\mathrm{rel}}(\tau, l^*)\right\rangle$ versus τ^2. The root mean square relative velocity $\Delta V_{\mathrm{rel}} = \sqrt{\langle \Delta V^2_{\mathrm{rel}}\rangle}$ determines the characteristic time scale of the motion, $\tau_{\mathrm{DAWS}} \equiv 1/[\sqrt{n}k\Delta V_{\mathrm{rel}}(l^*)]$, so that, with this definition, the field autocorrelation function can be written in a very simple way as $g_1(\tau) = \exp[-\frac{1}{6}\tau^2/\tau_{\mathrm{DAWS}}]$.

By varying the frequency, the scattering strength and hence also l^* was varied (see, for example, ref. [1]), enabling the relative particle velocity to be measured over a wide range of inter-particle distances $R = l^*$ inside the suspension. Figure 2(b) shows that at short distances, the relative particle velocity increases as the square root of distance, but that at longer distances it levels off to the value $\sqrt{2}V_{rms}$, where V_{rms} is the absolute rms particle velocity that can be measured directly in the single scattering regime using Dynamic Sound Scattering [6]. The saturation value $\sqrt{2}V_{rms}$ is the relative velocity of particles that move independently, indicating that all correlations in the motions become lost at large inter-particle separations. These observations can be summarized mathematically as follows:

$$\begin{aligned}\left\langle \Delta V^2_{rel}(l^*)\right\rangle &= \left\langle \left(\Delta\vec{V}(\vec{r}+l^*) - \Delta\vec{V}(\vec{r})\right)^2\right\rangle \\ &= 2\left\langle \Delta V^2\right\rangle - 2\left\langle \Delta\vec{V}(\vec{r}+l^*)\cdot\Delta\vec{V}(\vec{r})\right\rangle \\ &= 2\,V^2_{rms}\left(1 - C_V(l^*)\right)\end{aligned} \tag{5}$$

where

$$C_V(R) = \frac{\left\langle \Delta\vec{V}\left(\vec{r}+\vec{R}\right)\cdot\Delta\vec{V}(\vec{r})\right\rangle}{\langle \Delta V^2\rangle} = \exp[-R/\xi] \tag{6}$$

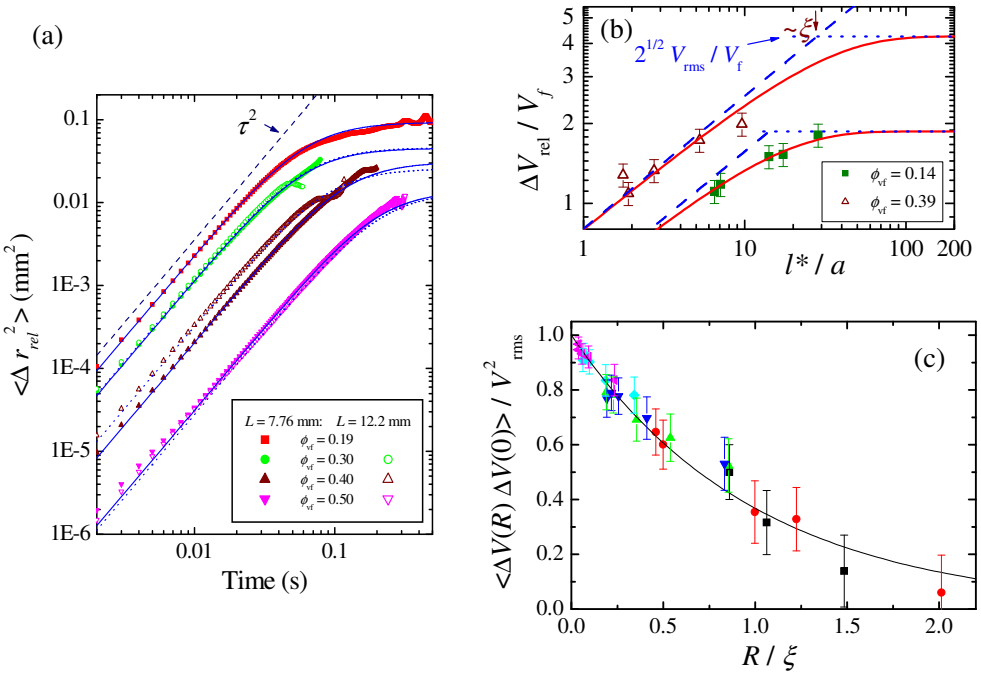

Fig. 2. – (a) Mean square relative displacement of glass beads in a fluidized suspension measured by Diffusing Acoustic Wave Spectroscopy. The data are plotted for several volume fractions of beads ϕ_{vf}, showing τ^2 behaviour indicative of ballistic particle motion at short times. (b) Root mean square relative velocity, divided by the fluidization velocity V_f, as a function of the ultrasound transport mean free path l^* normalized by the bead radius a. The mean free path l^* determines the average particle separation at which the velocity fluctuations are measured. The solid curves are fits of eq. 5, with C_V given by eq. 6, to the data for two volume fractions, enabling the particle velocity correlation length ξ to be measured at each volume fraction. (c) The particle velocity correlation function as a function of the average inter-particle separations $R = l^*$ at which the relative velocities are measured. The data show a good fit to the exponential function $\exp(-R/\xi)$, confirming the form of the correlation function that was assumed in (b). The different symbols represent data measured at different volume fractions of scatterers, with all the data collapsing onto a common curve when C_V is plotted as a function of R/ξ.

is the particle velocity correlation function, whose decay rate is determined by the velocity correlation length ξ. Equations 5-6 show how particle velocity correlation function can be determined from the relative velocity fluctuations measured in DAWS experiments, yielding the experimental results shown in fig. 2(c). The data in figs. 2(b) and (c) show that the assumed exponential decay of the velocity correlations with distance is consistent with observations, and enable the correlation length to be measured over a wide range of particle concentrations (with ϕ_{vf} varying from 0.08 to 0.50 in this case). The correlation length ξ measures the range of distances over which the particles move together, and

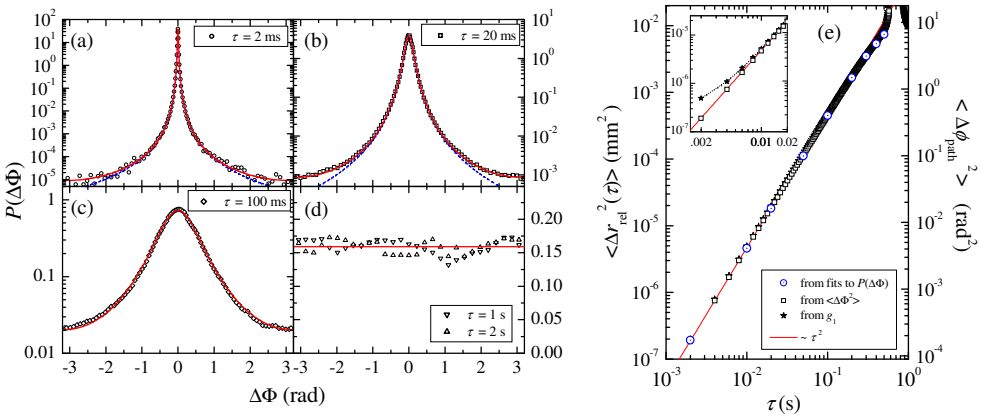

Fig. 3. – (a)-(d) The wrapped phase shift probability distribution $P(\Delta\Phi)$ at several time intervals τ. Experimental data are represented by the open symbols, and theoretical predictions by the solid curves. The dashed curves show the approximate expression for $P(\Delta\Phi)$ given by eq. 7. The only fitting parameter in the comparison of theory and experiment is the path phase variance $\left\langle \Delta\phi^2_{\rm path}(\tau) \right\rangle$ at each time τ, yielding a value of $\tau_{\rm DAWS}$ equal to 89 ms for these data. (e) Comparison of the relative mean square displacement of the particles determined from the phase data and from the field correlation function.

is an important quantity for understanding the physics of fluidized suspensions. Figure 2(c) also reveals a remarkable scaling of the velocity correlations for different particle concentrations when C_V is plotted as a function of R/ξ. Thus, Diffusing Acoustic Wave Spectroscopy can provide information on the dynamics of suspensions that is relevant both to fundamental studies of the motions in suspensions and turbulent fluids, and to practical applications such as monitoring mixing processes, the performance of chemical slurry bed reactors, and slurry flow in industrial processing.

By capitalizing on the ability of ultrasonic techniques to measure the phase and amplitude of the multiply scattered waves, DAWS has recently been extended to monitor system dynamics by analysing the fluctuations of the phase of the waves in time-varying systems [22]. Not only has this helped to advance our understanding of mesoscopic wave physics, where the role of phase for multiply scattered waves has often been ignored, but it has also provided a new approach for probing evolving media with increased sensitivity in some situations. Experimentally, the wrapped phase $\Phi(t,T) \in (-\pi : \pi]$ was extracted from the measured field at any evolution time T by a numerical technique that is equivalent to taking a Hilbert transform and obtaining the complex analytic signal $A(t,T)\exp\{i[\omega t + \Phi(t,T)]\}$. Information on the dynamics of the medium is contained in the phase difference over the time interval τ, $\Delta\Phi(\tau) = \Phi(T+\tau) - \Phi(T)$, which, since the phase difference is still a phase, is best represented between $-\pi$ and $+\pi$, and was therefore re-wrapped $\in (-\pi : \pi]$. To relate this phase difference to the particle dynamics, the relationship between the measured phase shift $\Delta\Phi(\tau)$ and the evolution of the path

phase $\Delta\phi_{\rm path}(\tau)$ was established. The simplest way to do this is via the wrapped phase difference probability distribution $P(\Delta\Phi(\tau))$, which can be calculated for random wave fields described by circular Gaussian statistics from the joint probability distribution of the fields at two times T_i and $T_j = T_i + \tau$ [22]. Results for the same fluidized suspensions of glass particles used for the data in fig. 2 are compared with theory in fig. 3(a)-(d), showing how the statistics of the phase difference evolve as the scatterers move, with the distribution becoming wider as the relative mean square displacement of the particles increases. At long times when the fields are no longer correlated, $P(\Delta\Phi(\tau))$ reaches a flat distribution. At short time intervals τ and small $\Delta\Phi$, $P(\Delta\Phi(\tau))$ has the simple form

$$P(\Delta\Phi) = \frac{1}{2}\frac{\langle\Delta\phi^2_{\rm path}\rangle}{\left[\langle\Delta\phi^2_{\rm path}\rangle + \Delta\Phi^2\right]^{3/2}}, \tag{7}$$

showing explicitly how the distribution depends on the path phase variance $\left\langle\Delta\phi^2_{\rm path}(\tau)\right\rangle$ and hence on the relative mean square displacement of the particles. While the general expression for $P(\Delta\Phi(\tau))$ is more complicated [22], it still only depends on one parameter, the path phase variance, allowing the excellent fits of theory and experiment shown in fig. 3 to accurately measure the mean square relative displacement of the particles. Figure 3(e) shows that measurements of $\left\langle\Delta r^2_{\rm rel}(\tau)\right\rangle$ from $P(\Delta\Phi)$ and g_1 are in superb agreement over a wide range of evolution time intervals τ, validating this phase method. The insert of this figure also shows an example where measurements of $P(\Delta\Phi)$ yields more accurate results. In this case, the presence of amplitude noise due to gain fluctuations degrades the field correlation measurements of the particle dynamics at short times, but has little effect on the phase statistics, which still give an accurate measurement of the particle motions.

Another way of characterizing the dynamics is to measure the variance of the wrapped phase difference $\left\langle\Delta\Phi^2(\tau)\right\rangle$. The variance of the measured phase shift is very different to the path phase variance $\left\langle\Delta\phi^2_{\rm path}(\tau)\right\rangle$, since the phase of the measured field is determined by the superposition of waves along all paths reaching the detector, while the path phase variance is determined by the fluctuations in the phase along a typical path (see eq. 1). Remarkably, a *universal relation* has been found between the wrapped phase variance and the path phase variance, as shown in fig. 4(a) by the solid curve. This universal relation means that the particle dynamics can be determined directly from the measured phase variance (open squares in fig. 3) – a simpler procedure than fitting the theoretical expression for $P(\Delta\Phi)$ to experimental data. Both methods work well for evolution times that are short enough that $\left\langle\Delta\Phi^2(\tau)\right\rangle$ is less than its upper limit of $\pi^2/3$, which occurs when $P(\Delta\Phi)$ has become flat.

Information on the dynamics can be followed to longer times by unwrapping the phase, removing the jumps of 2π to determine the evolution of the cumulative phase $\Phi_c(\tau)$. Here, as an example, we consider the cumulative phase shift variance, which is plotted as a function of $\tau/\tau_{\rm DAWS}$ in fig. 4(b). At early times, its increase with time is the same as the

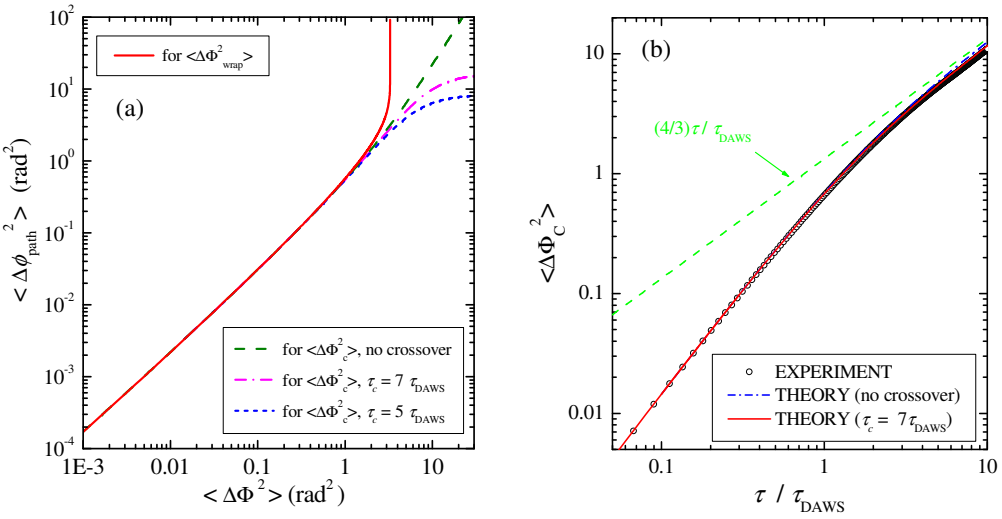

Fig. 4. – (a) Relation between the measured phase shift variance $\langle \Delta\Phi^2(\tau) \rangle$ and the path phase variance $\langle \Delta\phi^2_{\rm path}(\tau) \rangle$. For the wrapped phase, this relationship is universal (solid curve), while unwrapping the phase destroys the universality, giving the cumulative phase shift variance $\langle \Delta\Phi^2_c(\tau) \rangle$ greater sensitivity to the dynamics at long times. (b) The time dependence of the cumulative phase shift variance $\langle \Delta\Phi^2_c(\tau) \rangle$, showing a cross over to phase diffusion for times longer that $\tau_{\rm DAWS}$, with a phase diffusion coefficient that is influenced by the long-time dynamics.

.

wrapped phase variance, but at long times $\langle \Delta\Phi^2_c(\tau) \rangle$ becomes proportional to time, with $\langle \Delta\Phi^2_c(\tau) \rangle = D_\Phi \tau$, enabling the phase diffusion coefficient D_Φ to be measured. If the particles continue to move in ballistic trajectories at long times, $D_\Phi = 1/\tau_{\rm DAWS}$, but if the relative motion slows down, due to deviations from ballistic particle trajectories due to particle interactions, D_Φ is reduced. The solid curve in fig.4(b) shows a fit to a simple empirical crossover model [6], indicating that the characteristic time τ_c for such deviations to set in is about $7\tau_{\rm DAWS}$. An interesting general point to emerge from this analysis of the cumulative phase shift variance is that unwrapping the phase destroys the universal relationship between the measured phase variance and the path phase variance; this actually has a positive benefit since it gives the cumulative phase shift variance increased sensitivity to details of the particle motions at long times. The behaviour is shown by the dashed and dotted curves in fig. 4(a).

Another advantage of examining the phase statistics has been demonstrated by theory and experiment for the probability distributions of the phase derivatives with evolution time. These distributions have been determined for Φ', Φ'', Φ''' and found to be remarkably sensitive to early time dynamics, allowing the relative particle motions to be determined up to the 6th power in time - something that simply could not be achieved from measurements of the field correlation function. Another interesting quantity is the

cumulative phase correlation function, where current work is showing that, for evolving systems such as the bubbly liquids, the phase correlation function can be used to investigate motions at remarkably long times, beyond those accessible to field correlation measurements. Thus, progress in measuring and understanding the phase statistics and correlations of multiply scattered fields is continuing to advance the capabilities of Diffusing Acoustic Wave Spectroscopy for investigating the dynamics of strongly scattering materials.

3. – Probing food biomaterials with ultrasound

Many foods are heterogeneous on length scales that are comparable with the wavelengths of ultrasound in the 100 kHz to 10 MHz range, making ultrasonic spectroscopy of food materials a promising approach for investigating their mechanical properties, structure and dynamics. Because both scattering and dissipation of ultrasound are generally strong in such materials, most information on their properties comes from ballistic velocity and attenuation measurements. In this section, I focus on one example, bread dough, which contains one of the strongest scatterers of ultrasound, namely bubbles, with the bubbles being dispersed in a viscoelastic matrix, which contributes to the ultrasonic absorption. Thus, the physics of how ultrasound propagates in dough is remarkably rich. Understanding the effect of bubbles on the properties of dough is also critical to controlling the texture of bread, and hence its quality. As a result, ultrasonic characterization of bubbles in bread dough is potentially important to the food industry.

Ultrasonic experiments on bread dough reveal different properties as the frequency is varied [10, 11, 12, 13, 14, 15, 16, 17, 18, 19]. Indeed, there are three important frequency regimes. These are identified in fig. 5, which shows experiment and theory for the ultrasonic attenuation and phase velocity in bread dough over almost three decades in frequency. At low frequencies, $f < 100$ kHz, bubbles in dough drastically reduce the sound velocity, due to the large compressibility of the bubbles. There is excellent sensitivity to the presence of bubbles but no information on their sizes. The attenuation is relatively low in this frequency regime, making experiments easier. For frequencies between 100 kHz and 8 MHz, there is a strong resonant interaction between the ultrasonic waves and the bubbles, leading to a very large variation in the velocity and attenuation. Their frequency dependence at these intermediate frequencies depends on the bubble sizes, raising the interesting possibility of extracting information on the bubble size distribution in this opaque medium from ultrasonic measurements. At high frequencies, $f > 8$ MHz, the ultrasonic attenuation and velocity depend on matrix properties only, enabling structural relaxations of the molecular ingredients of the matrix to be probed.

The sensitivity of ultrasound to the concentration of bubbles in the low frequency regime (at $f \sim 50$ kHz) is shown in fig. 6. The dough samples were prepared by mixing together a strong Canadian breadmaking flour (CWRS), salt and water, to produce a lean-formula mechanically developed dough [23]. For these experiments, the bubble concentration was adjusted by varying the headspace pressure during mixing. As the bubble concentration is increased, the ultrasonic velocity drops dramatically, reaching

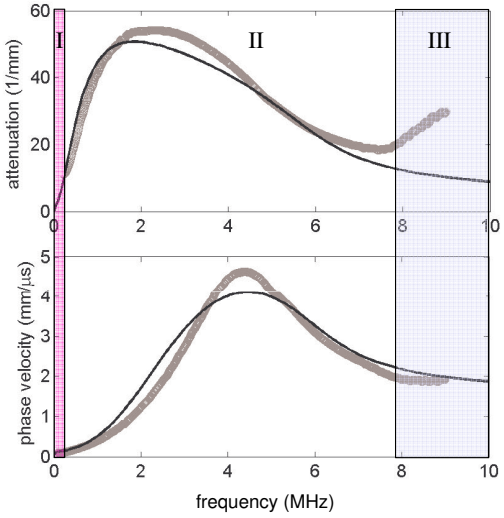

Fig. 5. – The ultrasonic attenuation and phase velocity as a function of frequency up to 10 MHz for a typical dough sample with a bubble concentration of 12%. The roman numerals and boxes indicate the three frequency regimes, as discussed in the text.

values less than the velocity of sound in air for concentrations above 2%. This behaviour can be understood qualitatively in the Wood's approximation for the low frequency compressibility of a bubbly liquid. In this approximation, the average compressibility of the sample $\kappa_{\rm s}$ is simply the volume-fraction-weighted average of the compressibilities of the bubble inclusions i and surrounding matrix m

$$\kappa_s = \phi_{\rm vf}\kappa_i + (1-\phi_{\rm vf})\kappa_m \tag{8}$$

where $\phi_{\rm vf}$ is the volume fraction of bubbles. Thus, since phase velocity and compressibility are related by $v = \sqrt{1/\rho\kappa}$, where ρ is the density,

$$\frac{1}{\rho_s v_s^2} = \frac{\phi_{\rm vf}}{\rho_i v_i^2} + \frac{1-\phi_{\rm vf}}{\rho_m v_m^2} \tag{9}$$

and the average sound velocity for concentrations of bubbles in this range reduces approximately to

$$v_s \approx v_{\rm air}\sqrt{\frac{\rho_{air}}{\rho_s\phi_{\rm vf}}}. \tag{10}$$

The density ratio in the square root factor in this expression shows why the velocity

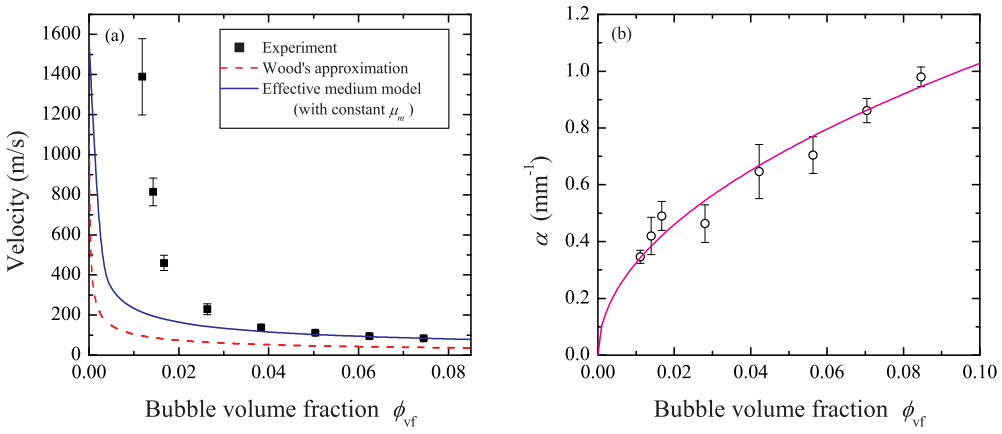

Fig. 6. – The ultrasonic velocity (a) and attenuation (b) in bread dough as a function of bubble volume fraction at 50 kHz.

is so much less than the velocity in air (340 m/s); the effective medium behaves as a material with the low compressibility of air, but with a larger density. For dough, this approximation underestimates the velocity at all volume fractions because it neglects the shear modulus of the dough matrix, which can be included in a more complete (but also more complicated) effective medium model [24]. For the higher volume fractions, where the complex shear modulus $\mu_m = 0.39 + i0.14$ MPa can be reasonably extrapolated from existing lower frequency shear rheology data on dough prepared at ambient pressure [14]; this model gives excellent agreement with experiment. At lower concentrations, however, the measured velocities are larger than this prediction, suggesting that the shear modulus of the dough matrix increases at low volume fractions. Thus the presence of bubbles in the dough enables the shear properties of the dough to be investigated using longitudinal waves - a considerable advantage as longitudinal ultrasonic measurements are easier to perform in lossy materials such as dough.

As shown in fig. 6(b), the ultrasonic attenuation increases as the square root of the volume fraction in this low frequency regime, a frequency dependence which is predicted by effective medium theories (solid line) [24, 16]. By treating the interaction of ultrasound with bubbles in a viscoelastic medium, it can be shown, at frequencies well below the resonance frequency ω_0 of the bubbles, that the attenuation is predicted to have the form:

$$\alpha = \sqrt{\frac{3\phi_{\mathrm{vf}}}{a^2}}\frac{\omega^2\Gamma}{\omega_0^3} \tag{11}$$

Here a is the radius of the bubbles, and Γ is the damping rate, which at low frequencies depends on viscous losses and thermal dissipation. If viscous losses dominate, the

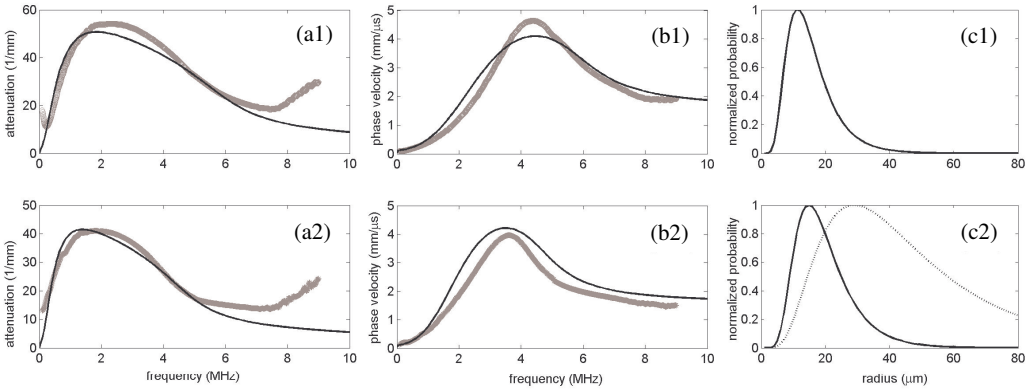

Fig. 7. – Frequency dependence of the ultrasonic attenuation (a1),(a2) and velocity (b1),(b2), showing the broad spectral features characteristic of resonant interactions with bubbles. The grey curves represent experimental data, and the solid black curves are theoretical predictions of the model outlined in the text. (See ref. 16 for more information.) The numbers (1) and (2) identify the times after mixing at which the data were taken: 53 minutes for (1) and 90 minutes for (2). The solid curves in (c1) and (c2) are the bubble size distributions inferred from the ultrasonic data at these two times. The dotted curve in (c2) are the results of x-ray tomography measurements.

dependence of α on bubble size in eq. 11 cancels out, since $\Gamma_{\text{viscous}} = 4\mu''/\rho\omega a^2$ and the resonant frequency of the bubbles depends inversely on the bubble radius, $\omega_0 \propto a^{-1}$. Thus, in this regime, the attenuation is sensitive only to the amount of gas entrained in the bubbles, and not on how the gas is distributed, providing a good indicator of the amount of gas entrained in the dough.

The sensitivity of these low-frequency measurements to bubble concentration is enabling the ultrasonic velocity and attenuation to be used to monitor dough mixing, where reliable methods of determining optimum mixing conditions are of considerable value [18]. For doughs prepared with leavening agents, ultrasonic velocity and attenuation can be used to monitor the growth of the bubbles due to incorporation of CO_2 [12]. Low frequency velocity measurements can also be used to assess dough quality [25], and since these ultrasonic measurements can be performed on small samples, such measurements are potentially very useful in wheat breeding programs.

At intermediate frequencies, the resonant coupling of ultrasound with the bubbles causes the attenuation and phase velocity to exhibit a large frequency dependence, with broad peaks that contain information on the bubble size distribution (fig. 7). To interpret the experimental data, Leroy et al. [16] have used a model that extends the well-established model for the resonant interactions of sound with bubbles in liquids [26, 27, 28] to viscoelastic materials, by incorporating a simple correction to the resonant frequency proposed by Alekseev and Rybak [29]. Physically, the effects of finite shear rigidity are to shift the resonant frequency to higher frequencies and also to weaken the resonance. This model has been tested on transparent agar gels, where the bubble sizes can be measured

optically, and found to describe the data well [16]. Applying the same model to dough, as described in ref. [16] and shown by the solid curves in figs. 7(a),(b), the bubble size distribution can be estimated. The inferred bubble size distributions at two times after mixing are shown in fig. 7(c). At the later time, the evolution of the size distribution had slowed down sufficiently to enable bench-top x-ray tomography measurements to independently measure the size distribution (dotted curve in fig. 7(c)) [15]. This comparison indicates that the analysis of the ultrasonic data estimates smaller bubble sizes than the x-ray measurement, although comparison between results is not straightforward because the conditions of sample preparation were not the same in both cases. Work is continuing to understand the origin of this discrepancy, so that the ultrasonic technique can be developed to unambiguously determine bubble sizes. Since ultrasonic measurements can be performed quickly, potentially even online, this information has practical relevance for monitoring dough quality during breadmaking. Even though questions remain to be resolved concerning the absolute sizes of the bubbles determined from the ultrasonic velocity and attenuation, the shift of the resonance features in the ultrasonic data to lower frequencies at the later observation time shows the effects of disproportionation in the dough due to Ostwald ripening; this phenomenon leads to an increase in the average size of the bubbles with time as gas diffuses from the smaller bubbles to the larger ones [30]. Such information on the dynamics of the bubbles in bread dough is valuable for understanding the evolution of the bubble structure.

Measurements of ultrasonic velocity and attenuation in dough in the high frequency range (above the bubble resonance regime, $f > 8$ MHz) reveal information on matrix properties. The frequency dependence of the data show signatures of ultrasonic relaxation phenomena, which can be interpreted using a molecular relaxation model [33, 34]. Different fast relaxation times were observed for ambient-mixed dough (5 ns) and vacuum-mixed dough (1 ns) [31]. These relaxation times may be associated with conformational rearrangements in glutenin - the supermolecular structure of proteins in the gluten matrix - perhaps due to the loop-to-train transition that is thought to play a role in the elasticity of glutenin [32]. Thus data in this frequency range can probe ultrasonic stress-induced changes in the secondary structure of gluten proteins that are important for understanding the viscoelastic properties of this complex food material.

This example of ultrasonic spectroscopy shows that both ultrasonic velocity and attenuation are sensitive probes of the gas cell structure of bread dough, enabling new approaches to optimizing loaf quality to be developed. Ultrasound can be used to follow the evolution of the gas cells (bubbles) throughout the entire breadmaking process, from the initial entrainment of gas bubbles in dough during mixing, though the expansion of the gas cells during proofing, all the way up to the final foam structure of bread. Ultrasound can also be used to probe changes in the viscoelastic properties of the dough matrix. Remarkably, despite the complexity of dough and bread as mesoscopic materials, their mechanical properties can be elucidated using relative simple physics models. This combination of factors is leading to a new awareness of ultrasound's potential to provide novel information on technical issues of importance to the cereals processing industry.

4. – Conclusions

Ultrasonic spectroscopy is both contributing to and capitalizing on advances in the wave physics of complex mesoscopic materials. As a result, new approaches that exploit the advantages of ultrasonic techniques are being developed to characterize the structure and dynamics of this increasing important class of materials. This paper has discussed two examples. The first was Diffusing Acoustic Wave Spectroscopy, which is a sensitive technique for monitoring changes in materials in which conventional imaging techniques are impossible due to multiple scattering, and which is complementary to Diffusing Optical Wave Spectroscopy. DAWS is based on direct measurements of the field autocorrelation function, and has been extended recently to probe dynamics using the phase of multiply scattered waves. This approach has some advantages practically, as well as being a way of advancing our understanding of phase in mesoscopic wave physics. In this paper, the application of this technique to the investigation of particulate and bubbly suspensions was demonstrated, but many more applications of this technique can be envisaged (e.g., in process control).

The second example considered here was the characterization of biological materials of importance in food science. Many such materials have internal length scales that are comparable with the wavelength of ultrasound, making ultrasonic spectroscopy a particularly relevant approach. The studies of bread dough that were summarized in this paper demonstrate how advances in physics underpin practical applications. The latter are of considerable economic potential in the rapidly growing functional foods area, where the interaction of functional ingredients with the bubble structure can damage the taste and appearance of food products unless remedial action is taken. By monitoring the properties at an early stage in production and helping to understand the dynamics of these interactions, ultrasonic techniques can help overcome such problems.

* * *

I would like to thank the many students and colleagues who have contributed to the research that has been reviewed in this paper. Support from NSERC is also gratefully acknowledged.

REFERENCES

[1] Page J.H., this volume, p. 75.
[2] Page J.H., Schreimer H.P., Bailey A.E. and Weitz D.A., *Phys. Rev. E*, **52** (1995) 3106.
[3] Page J.H., Sheng P., Schreimer H.P., Jones I., Jing X. and Weitz D.A., *Science*, **271** (1996) 634.
[4] Schreimer H.P., Cowan M.L., Page J.H., Sheng P., Liu Z. and Weitz D.A., *Phys. Rev. Lett.*, **79** (1997) 3166.
[5] Cowan M.L., Beaty K., Page J.H., Liu Z and Sheng P, *Phys. Rev. E*, **58** (1998) 6626.
[6] Cowan M.L., Page J.H. and Weitz D.A., *Phys. Rev. Lett.*, **85** (2000) 453.
[7] Cowan M.L., Jones I.P., Page J.H. and Weitz D.A., *Phys. Rev. E*, **65** (2002) 066605.

[8] Cowan M.L., Page J.H., Weitz D.A. and van Tiggelen B.A., in *Wave Scattering in Complex Media: From Theory to Applications*, edited by van Tiggelen B.A. and Skipetrov S.E. Kluwer Academic Publishers: NATO Science series, Amsterdam 2003, pp. 151-174.
[9] Snieder R. and Page J., *Physics Today*, **60(5)** (2007) 49.
[10] Létang C., Piau M., Verdier C., and Lefebvre L., *Ultrasonics*, **39** (2001) 133.
[11] Elmehdi H.M., *Ph.D. Thesis*, University of Manitoba 2001.
[12] Elmehdi H.M., Page J.H. and Scanlon M.G., *Trans. Inst. Chem. Eng. Part C: Food Bioprod. Proc.*, **81** (2003) 217.
[13] Elmehdi H.M., Page J.H. and Scanlon M.G., *J. Cereal Sci.*, **38** (2003) 33.
[14] Elmehdi H.M., Page J.H. and Scanlon M.G., *Cereal Chem.*, **81** (2004) 504.
[15] Bellido G.G., Scanlon M.G., Page J.H. and Hallgrimsson B., *Food Research International*, **39** (2006) 1058.
[16] Leroy V., Fan Y., Strybulevych A.L., Bellido G.G., Page J.H.. and Scanlon M.G., in *Bubbles in Food 2: Novelty, Health and Luxury*, edited by Campbell G.M., Scanlon M.G. and Pyle D.L., AACC Press, St Paul, MN 2008 pp. 51-60.
[17] Scanlon M.G., Page J.H. and Elmehdi H.M., in *Bubbles in Food 2: Novelty, Health and Luxury*, edited by Campbell G.M., Scanlon M.G. and Pyle D.L., AACC Press, St Paul, MN 2008 pp. 217-230.
[18] Mehta K.L., Scanlon M.G., Sapirstein H.D. and Page J.H., *J. Food Science*, **74** (2009) E455.
[19] Leroy V, Pitura K.M., Scanlon M.G. and Page J.H., *J. Non-Newtonian Fluid Mechanics*, **165** (2010) 475.
[20] Maret G. and Wolf P.E., *Z. Phys. B*, **65** (1987) 409
[21] Pine D.J., Weitz D.A., Chaikin P.M. and Herbolzheimer E., *Phys. Rev. Lett.*, **60** (1988) 1134.
[22] Cowan M.L., Anache-Ménier D., Hildebrand W.K., Page J.H. and van Tiggelen B.A., *Phys. Rev. Lett.*, **99** (2007) 094301.
[23] Preston K.R., Kilborn R.H. and Black H.C., *Can. Inst. Food Sci. Technol. J.*, **15** (1982) 29.
[24] Sheng P., in *Homogenization and Effective Moduli of Materials and Media*, edited by Ericksen J.L., Kinderlehrer D., Kohn R. and Lions J.-L. Springer 1988 p. 196.
[25] Scanlon M.G., Mehta K.L., Elmehdi H.M. and Page J.H., unpublished.
[26] Foldy L.L., *Phys. Rev.*, **67** (1945) 107.
[27] Leighton T.G., *The Acoustical Bubble* Academic Press, London 1994.
[28] Prosperetti A., *J. Acoust. Soc. Am.*, **61** (1977) 17.
[29] Alekseev V.N. and Rybak S.A., *Acoustical Physics*, **45** (1999) 535.
[30] Van Vliet T., in *Bubbles in Food*, edited by Campbell G.M., Webb C., Pandiella S.S. and Niranjan K. Eagan Press: St. Paul, MN. 1999, pp. 121-127.
[31] Scanlon M.G., Page J.H., Leroy V., Fan Y. and Mehta K.L., in *Proc. 5th International Symposium on Food Rheology and Structure*, edited by Fischer P., Pollard M. and Windhab E.J. ETH Zurich 2009, pp. 378-381.
[32] Belton P. S., *J. Cereal Sci.*, **29** (1999) 103.
[33] Litovitz T.A., and Davis C.M., in *Physical Acoustics*, Vol IIA, edited by Mason W.P. Academic Press, New York 1965 pp. 282-350.
[34] Marvin R.S. and McKinney J.E., in *Physical Acoustics*, Vol IIB, edited by Mason W.P. Academic Press, New York 1965 pp. 160-230.